

RSC Advances

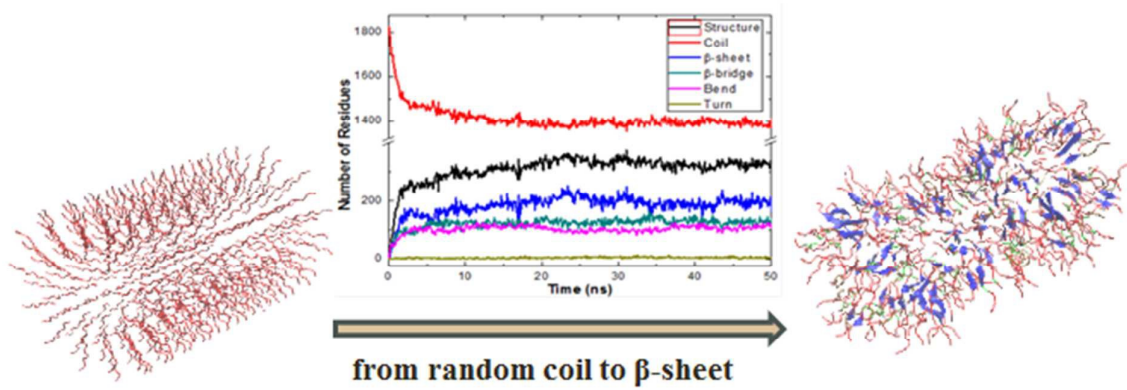


This is an *Accepted Manuscript*, which has been through the Royal Society of Chemistry peer review process and has been accepted for publication.

Accepted Manuscripts are published online shortly after acceptance, before technical editing, formatting and proof reading. Using this free service, authors can make their results available to the community, in citable form, before we publish the edited article. This *Accepted Manuscript* will be replaced by the edited, formatted and paginated article as soon as this is available.

You can find more information about *Accepted Manuscripts* in the [Information for Authors](#).

Please note that technical editing may introduce minor changes to the text and/or graphics, which may alter content. The journal's standard [Terms & Conditions](#) and the [Ethical guidelines](#) still apply. In no event shall the Royal Society of Chemistry be held responsible for any errors or omissions in this *Accepted Manuscript* or any consequences arising from the use of any information it contains.



MOLECULAR DYNAMICS SIMULATIONS OF SELF-ASSEMBLED PEPTIDE AMPHIPHILE BASED CYLINDRICAL NANOFIBERS

E. Deniz Tekin

University of Turkish Aeronautical Association, Ankara 06990, Turkey.

edtekin@thk.edu.tr

ABSTRACT

We carried out united-atom molecular dynamics simulations to understand the structural properties of peptide amphiphile (PA)-based cylindrical nanofibers and the factors that play a role in the "Self-Assembly" process on some specific nanofibers. In our simulations, we start from various cylindrical nanofiber structures with different number of layers and different number of PAs in each layer, based on previous experimental and theoretical results. We find that the 19-layered nanofiber, with 12 PAs at each layer, distributed radially and uniformly with alkyl chains in the center, is the most stable configuration with a diameter of 8.4 nm which is consistent with the experimental results. The most dominant secondary structures formed in the fibers are random coils and β -sheets, respectively. We also find that hydrophobic interactions between the VVAG-VVAG moiety of the PA molecules and electrostatic interactions between D- Na^+ and between E-R are responsible for fiber's self-assembly properties. During the aggregation process, first dimers, then trimers are formed.

KEYWORDS: Molecular dynamics simulations, odd-even effect, self-assembly, peptide amphiphiles, nanofiber.

INTRODUCTION

Recently [1], energy minimization simulations revealed the existence of an “odd-even effect” in self-assembled peptide amphiphiles (PAs) that form a cylindrical nanofiber. This odd-even effect can be summarized as follows: Minimum energy configuration of a nanofiber formed by an odd (even) number of layers is achieved if each layer has even (odd) number of PAs that are radially and uniformly located with alkyl chains in the center of the cylinder. To be able to conclude the emergence of this odd-even effect, many simulations have been done for many different number of layers and different number of PAs at each layer. In the current work, we continue with our investigations on some specific odd and even-layered nanofibers chosen from the minimum energy configurations found in [1] and study their stability to understand the role of molecular interactions. Before we describe our results and derive conclusions in the self-assembled cylindrical nanofibers based on PAs, let us briefly recapitulate the relevant literature both in the experimental and the computational sides.

Self-assembly mechanism is ubiquitous in the Universe almost in any organization at the macroscopic and microscopic scales, ranging from galaxies to molecules. Molecular self-assembly is due to various attractive and repulsive forces such as van der Waals, electrostatic, hydrogen bonding, hydrophobic and stacking interactions. These interactions lead to supra-molecular structures combining the individual molecules. It has been an active area of research to use the self-assembly mechanism to produce new, well-defined functional nanoscale materials such as nanotubes, nanofibers, nanoparticles, gels and nanorods [2-5]. Among all the organic molecules, self-assembly of PA molecules in water, under physiological conditions into effectively one dimensional cylindrical nanofibers and eventually to hydrogel, has a great interest because of their biocompatibility and bioactivity which make them suitable to be used in different biomedical applications such as drug delivery, regenerative medicine and tissue reparation [6-13]. The PA molecule is amphiphilic with its hydrophobic alkyl chain and a hydrophilic peptide segment. Experimental synthesis of PAs follows the similar routine of standard peptide-based systems with the additional alkyl tail which gives a greater mechanical control. Self-assembled PAs can assume various shapes and conformations that determine their functionality [14, 15].

Experimental studies have been conducted to examine various aspects of self-assembling PAs and PA-based nanofibers. Characterizations of PAs are usually carried out with visual techniques such as transmission and scanning electron microscopy, and with other techniques such as mass spectroscopy, Fourier transform-infrared spectroscopy, Raman spectroscopy, rheology and circular dichroism spectroscopy (CD). Paramonov *et al.* [16] prepared a series of 26 PA derivatives to study the importance of hydrogen bonding in the self-assembly mechanism of PA based nanofibers. They reported the formation of β -sheet hydrogen bonds by four amino acids closest to the core of the

nanofiber. Cylindrical nanofiber is not formed if these hydrogen bonds disappear. These results were confirmed by another experimental work carried out by Jiang *et al.* [17] who studied the internal structure of self-assembled PA nanofibers using IR-spectroscopy and polarization modulation-infrared reflection-absorption spectroscopy. To understand the effects of charged groups on the self-assembling PA molecules on nanofiber formation, Toksoz *et al.* [18] designed and synthesized three PA molecules with different charges at physiological pH; Lys-PA (positively charged), His-PA (neutral) and Asp-PA (negatively charged). They showed that charge isolation and neutralization are important for the formation of nanofibers. The role of hydrophobic interactions on self-assembly mechanism of PA molecules was studied experimentally by changing the length of the alkyl tail [19, 20] and/or the amino acid sequence [21-23]. PA molecules, which have different lengths in their alkyl tails, form self-assembled nanostructures with a β -sheet conformation in different shapes and sizes at different pH values of the environment. An increase in the number of hydrophobic amino acid in the peptide segment of the PA molecules has a tendency to promote β -sheet structures and leads to the formation of long nanofibers with a high mechanical stiffness.

The quoted experiments above and many others that are not mentioned have had great successes [24-26] in the understanding of self-assembly mechanism of PAs, yet there are still many issues that need better understanding with the help of theoretical simulations. Currently, computational resources are quite advanced that certain phenomena which are too fast to understand in the experiments can be studied via molecular simulations. For example one could specifically study the effects of certain forces or factors by isolating them in a simulation an option which can be hard to do in an experiment. Such simulations could help experimentalists design nanofibers with desired properties.

Although, simulation of self-assembled PAs is a relatively new field, the computational techniques that are used are well-established in computational chemistry and physics. Here we shall use united atom Molecular Dynamics (MD) simulations to understand the structural properties of the PA-based cylindrical nanofibers.

Lee *et al.* simulated the self-assembly of PA molecules having the sequence of SLSLA AEIKVAV that form cylindrical fibers, using atomistic [27] and coarse-grained [28] MD simulations in water. The effect of peptide sequence on the secondary structure of PA-based cylindrical nanofibers was also studied, since it is believed that the stability of a cylindrical fiber is due to the β -sheet secondary structure. For this purpose, Lee *et al.* [29] simulated two different PA sequences which differ in number of valine and showed that the PA with more valine has a higher population of β -sheet structure and hydrogen bonds.

Velicho *et al.* [30] suggested that self-assembly of PA molecules are due to the hydrophobic interactions between alkyl tails and the inter-peptide hydrogen bonds. But they neglected the electrostatic interactions. Fu *et al.* [31] also studied the role of hydrophobic interactions on the self-assembly of PA molecules by a novel coarse-grained MD simulation, systematically changing the model parameters of the hydrophobic interactions, and found that as the hydrophobic interaction increases, cylindrical nanostructures containing either β -sheets or random coils form.

Understanding the self-assembly mechanism of the PA molecules and the related noncovalent interactions are important in structural biochemistry to design new PAs and PA-based materials for biomedical applications. In our simulation, we start from a cylindrical nanofiber structure based on the results of the recent experimental [7, 17, 32] and theoretical works [1, 27, 33-35] to study the stability of the fibers and forces (interactions) which bring/hold them together.

COMPUTATIONAL DETAILS

The PA molecule contains a hydrophobic alkyl chain (C_{12}) covalently attached to the N-terminus of the sequence VVAGERGD (Figure 1a). These PA molecules were synthesized by Guler group using solid phase fluorenylmethoxycarbonyl (Fmoc) peptide synthesis method [4]. In [1], the PA molecule was prepared at pH7. In what follows we shall use the results of that work. The total net charge of the PA molecule is -2 with charges as: E= -1, R= +1 and D= -2. The starting terminal of the peptide portion, that is *Valine*, was chosen as NONE (C_{12} will be attached to it) and the end terminus was selected as COO^- . Using this PA, the starting structures (Figure 1b shows one layer of the initial structure) and then cylindrical nanofibers were formed in various sizes (in total there are 126 structures) (Figures 1c and 1d).

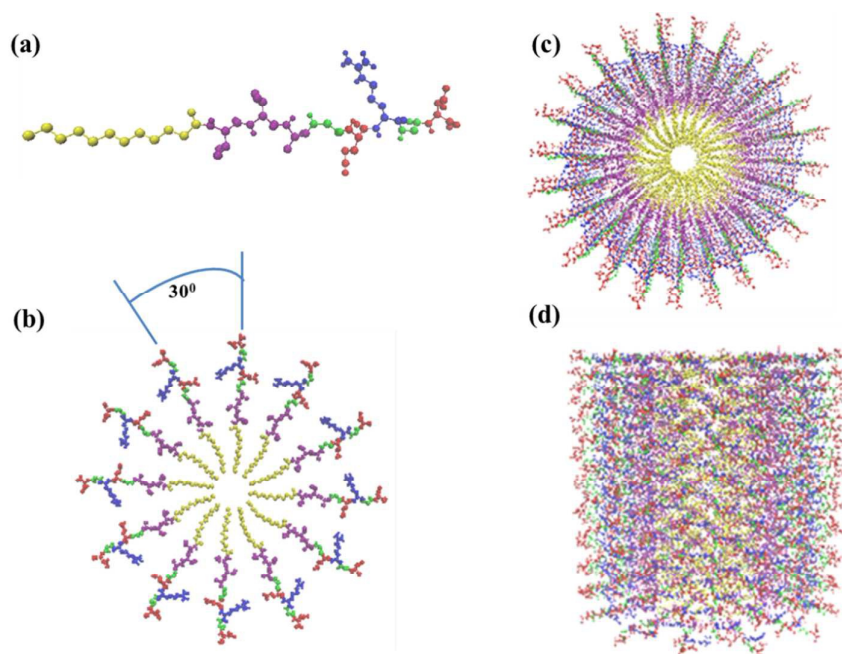


Figure 1. (a) One PA molecule prepared at pH7 where the PA sequence is C₁₂-VVAGERGD; acidic amino acids are in red, basic ones are in blue, non-polar ones are in purple, polar ones are in green and alkyl tails are in yellow. (b) Representative starting structure of 12 PA molecules are placed with a 30° angle to form the initial layer. The next layer is placed on the top of this layer rotated by half of the angle between the PAs. (c) Front and (d) side view of 19-layered nanofiber formed by GROMACS, there are 19x12 = 228 PAs in total.

Here, we choose some of the structures (see Table 1) with minimum energy from [1]. Each structure is solvated with SPC type water molecules [36] in a rhombic dodecahedron box. Periodic boundary conditions are used in the simulations. Counter ions (Na⁺) are added to neutralize each system. A 1000-step energy minimization with the steepest-descent algorithm is applied to the solvated systems to ensure that the systems have an appropriate geometry. MD simulations are carried out using GROMACS 4.5.6 code [37] and GROMOS 53a6 [38] force field combined with Berger lipid parameters [39]. (Since the force fields that exist in the current literature are not defined for such mixed molecules, one should take such a path.)

Table 1: Details of simulations for 11 different choices of cylindrical nanofibers.

| # of layers | # of PA at each layer | Angle between the PAs | Total # of PA in a nanofiber | MD simulation length (ns) |
|-------------|-----------------------|-----------------------|------------------------------|---------------------------|
| 7 | 10 | 36° | 70 | 50 |
| 9 | 10 | 36° | 90 | 50 |
| 12 | 7 | 51.4° | 84 | 50 |
| 13 | 8 | 45° | 104 | 50 |
| 14 | 9 | 40° | 126 | 50 |
| 16 | 9 | 40° | 144 | 50 |
| 17 | 8 | 45° | 136 | 30 |
| 18 | 7 | 51.4° | 126 | 30 |
| 19 | 12 | 30° | 228 | 50 |
| 20 | 7 | 51.4° | 140 | 30 |
| 21 | 8 | 45° | 168 | 30 |

Each energy-minimized structure is then equilibrated with NVT and NPT ensembles to stabilize the temperature and pressure at 300 K and 1 bar, respectively. During the production dynamics, each structure is simulated for 30 ns or 50 ns using the NPT ensemble. Pressure is kept constant with a coupling time constant of 2.0 ps using an isotropic Parrinello–Rahman barostat [40]. Temperature is kept constant with a coupling time constant of 0.1 ps using a velocity rescaling thermostat [41]. To examine time-dependent trajectories, Newton's 2nd equation of motion is integrated with the Leap-frog algorithm for the time step of 2 fs. The linear constraint solver (LINCS) algorithm [42] is used to keep all bonds rigid. Particle Mesh Ewald (PME) method [43] is applied to calculate the long-range electrostatic interaction with a 0.16 nm grid width and a fourth order cubic interpolation. The short-range electrostatic and van der Waals interactions are described using the Verlet cut-off scheme [44] with a 1.0 nm cut-off radius and are updated every 10 time steps. Initial velocities are assigned randomly from the Maxwell distribution at 300 K. Coordinates and energies are recorded at every 10 ps for the trajectory analysis and no coordinates are constrained during the production run.

RESULTS AND DISCUSSIONS

After making necessary corrections (concatenation of the files and imposing periodicity) on trajectories obtained from the production MD simulations, Root Mean Square Deviation (RMSD) and the hydrogen bond analysis (Figure 2), Radius of Gyration (Rg) (Figure 3), secondary structure analysis (Figures 4, 5 and Figures S1, S2), hydrophobic (Figure 6 and Figure S3) and electrostatic interactions (Figure 7 and Figure S4) are carried out. Furthermore, representative snapshots are taken for each 10 ns of 30 or 50 ns simulations created via visual molecular dynamics [45] (Figure 8 and Figures S5-S14).

RMSD is calculated relative to the structure present in the energy-minimized initial configuration, that is the PA molecules at desired position forming a cylindrical nanofiber, and the equilibrated system after 50 *ns* MD simulation. An RMSD change less than or around 2 *nm* means that the biomacromolecule is intact and larger values mean that it disintegrates. The RMSD graphs (Figure 2) yield the conclusion that even-layered cylindrical nanofibers have stable configurations up to and including 16 layers with an RMSD value less than or around 2 *nm*, but they are unstable for 18 and 20 layers with an RMSD value larger than 2 *nm*. More specifically, for the 20-layered (18-layered) nanofiber, it is observed that the RMSD value increases with time and reaches to 6 *nm* (4 *nm*). And also, the snapshots (Figure 8 and Figures S5-S14) of the 18 and 20-layered systems show that after a certain time (about 5 *ns*), the systems start to disintegrate. For the 16-layered nanofiber, although there is no disintegration with time, the RMSD value is slightly above 2 *nm*. But for odd-numbered cylindrical nanofibers, such a generalization cannot be made. For 7, 9 and 13-layered nanofibers the RMSD values are below 2 *nm*. As for the 17 and 21-layered nanofibers, in a short amount of time (1-2 *ns*), the RMSD value rises above 2 *nm* and the systems begin to break up. But, the 19-layered nanofiber remains in equilibrium around a value less than 2 *nm* during the simulation. That is, the initially formed 19-layered cylindrical nanofiber still retains its initial conformation at the end of the simulation.

To summarize the results of the snapshots and the RMSD graphs, let us note that at the end of the 50 *ns* simulation, while 7, 9 and 12-layered fibers (Figure 2a and Figures S5-S7) take the form of a micelle, 13, 14, 16 and 19-layered fibers (Figure 2b, Figure 8 and Figures S8-S10) are still cylindrical nanofibers. The other fibers with 17, 18, 20, 21 (Figure 2c and Figures S11-S14) layers break up to two or more pieces within a very short period of time (0.5-1.0 *ns*). These results suggest that the number of PAs in each layer and the number of layers in a cylindrical nanofiber determine the stability or instability of the fiber in a rather non-trivial way. For example, there are 8 PAs in each layer of the 17 and 21-layered nanofibers and there are 7 PAs in each layer of 18 and 20-layered nanofibers. These systems are unstable. 19-layered nanofiber, however, has 12 PAs in each layer and the system is stable.

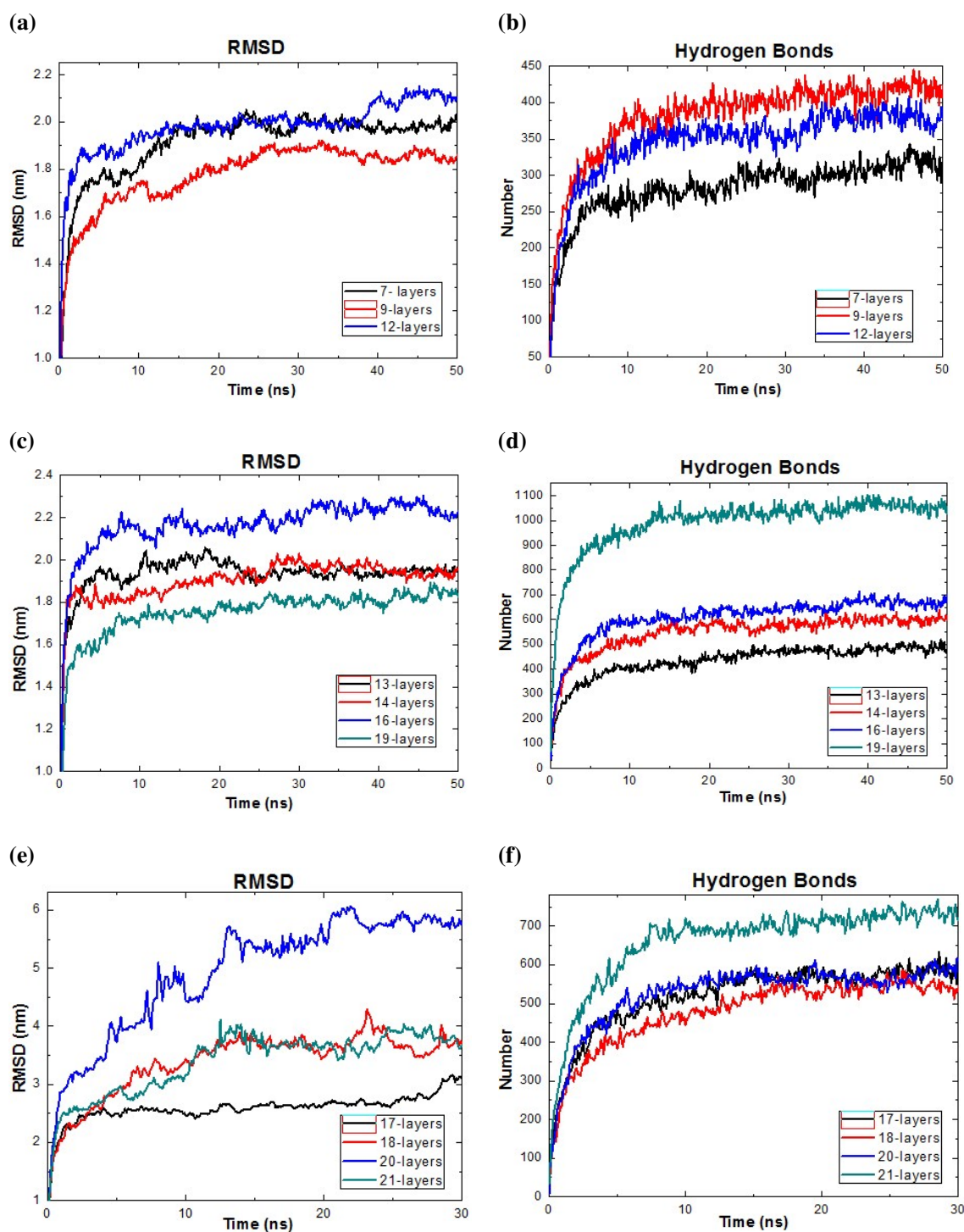


Figure 2. Plots of the RMSD of the backbone atoms of the PA-based cylindrical nanofibers vs. the starting structure and plots of the number of inter-molecular hydrogen bonds within 0.35 nm for (a-b) 7, 9 and 12-layered nanofibers (c-d) 13, 14, 16 and 19-layered nanofibers (e-f) 17, 18, 20 and 21-layered nanofibers during the simulation time.

It is also observed that there is a relationship between the number of hydrogen bonds (Figure 2) and the RMSD values. For the fibers which have RMSD values below or around 2 *nm*, there is an increase in the number of hydrogen bonds over time. For example, during the simulation, although the number of hydrogen bonds in the 16-layered structure (RMSD~2.0 *nm*) (Figure 2d) is more than 600, in the 18-layered nanofiber (RMSD>3.0 *nm*) (Figure 2e) that number is around 500. This result is not related to the total number of PAs in the nanofibers, but it is related to the number of PAs in each layer. For example, when the 14 and 18-layered structures are compared, although each structure has 126 PA molecules, there are approximately 600 hydrogen bonds in the 14-layered nanofiber (RMSD<2.0 *nm*) but there are approximately 500 hydrogen bonds in the 18-layered nanofiber (RMSD>3.5 *nm*).

To see the changes in the total size of the structures, the radius of gyration (*R_g*) of the nanofiber during the 50 *ns* simulation time is calculated (Figure 3). The analysis shows that the *R_g* results support the RMSD results. Namely, while in the 17, 18, 20 and 21-layered structures (Figure 3c), the value of *R_g* is increasing with time, in the other layers (Figures 3a and 3b), there are two regions in the *R_g* graphs: A rapid collapse of the structure, that is, the value of *R_g* decreases with time and then maintains an almost constant value. That means these structures are more compact than the 17, 18, 20 and 21-layered structures. Another important observation is that in the 19-layered structure, unlike in the other structures, the *R_g* value does not show a considerable drift: It starts from 4.3 *nm* and drops to the constant value of 4.1 *nm*. According to the *R_g* computation, the 19-layered structure has a diameter of (about) 8.4 *nm* which is consistent with the results of the experiments [7, 21].

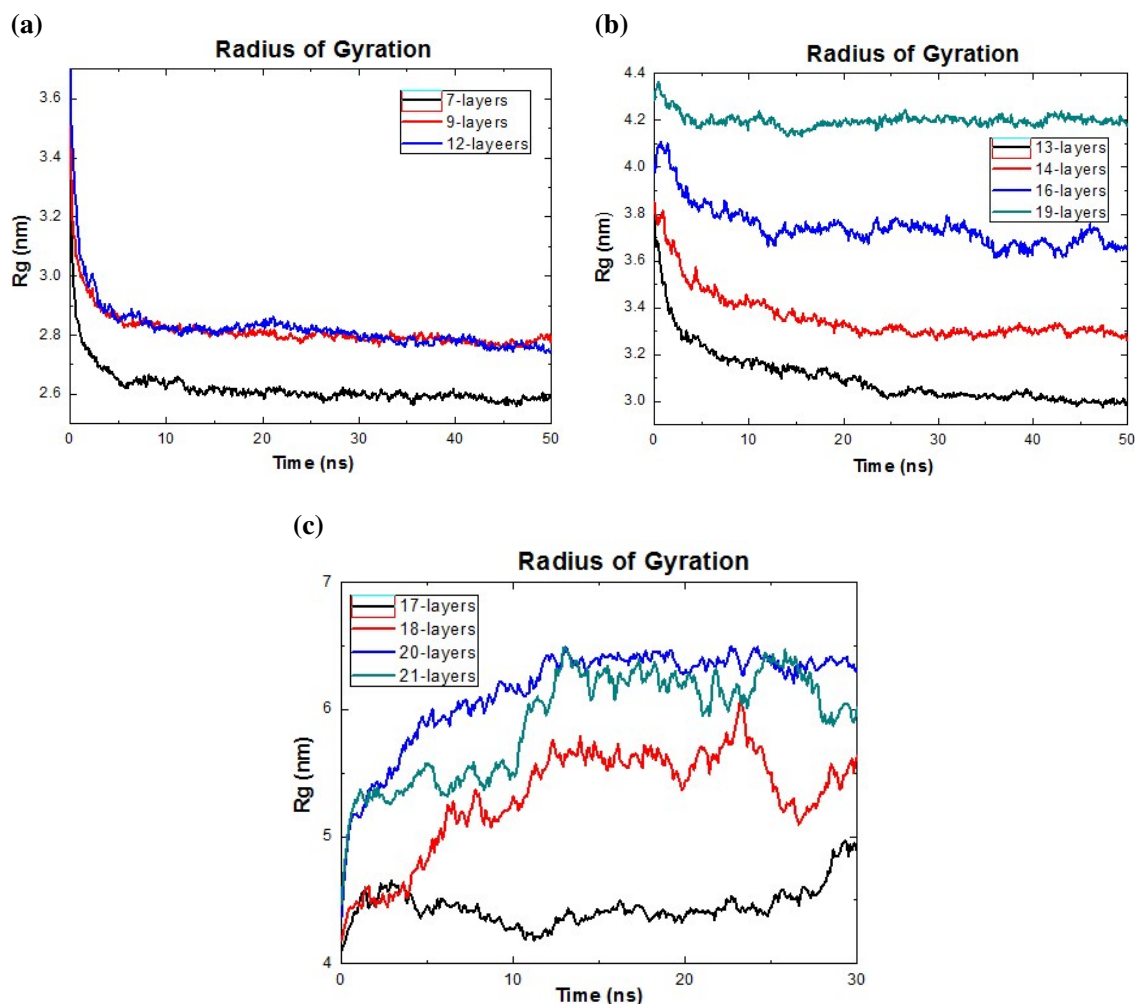


Figure 3: Plots of the Radius of Gyration for (a) 7, 9 and 12-layered nanofibers (b) 13, 14, 16 and 19-layered nanofibers (c) 17, 18, 20 and 21-layered nanofibers over the simulation time.

The cause of the collapse of the structures is probably due to the secondary structure changes. Dictionary of Secondary Structure of Proteins (DSSP) program by Kabsch and Sander [46] is used to calculate the secondary structure (*i.e.* helix, sheet, turn *etc.*) changes of each fiber as a function of simulation time (Figure 4 and Figure S1). In our simulation, for each nanofiber, the most dominant secondary structure is the random coil (between 64-70%) during the simulation time. This is an expected result: Guler *et al.* [4] observed that the PA solution at pH 7 had a mostly random coil structure using CD spectra and similarly, Behanna *et al.* [6] found that the CD spectra of two PAs with a triple Glu sequence, which have a negative net charge, showed a random coil secondary structure. Furthermore, for all sequences, while the ERGD part adopts the random coil region, mostly VV, VA or VVAG parts, which are close to the alkyl tail, adopt a β -sheet structure. Thus, the second most dominant secondary structure is the β -sheet (between 5-14%) in all nanofibers. The 19-layered

nanofiber has the highest number of β -sheet structure (Figure 5). (See Figure S2 for the β -sheet populations of the other structures.) The same result can also be seen from the h-bonding analysis: Maximum number of hydrogen bonds exist in the 19-layered fiber and exceeds 1000. The increase of the hydrogen bonds over time is an evidence of the formation of the β -sheets. This result is consistent with some theoretical and experimental studies, that is the stability of a cylindrical fiber is due to β -sheet secondary structure [16, 17, 27, 28].

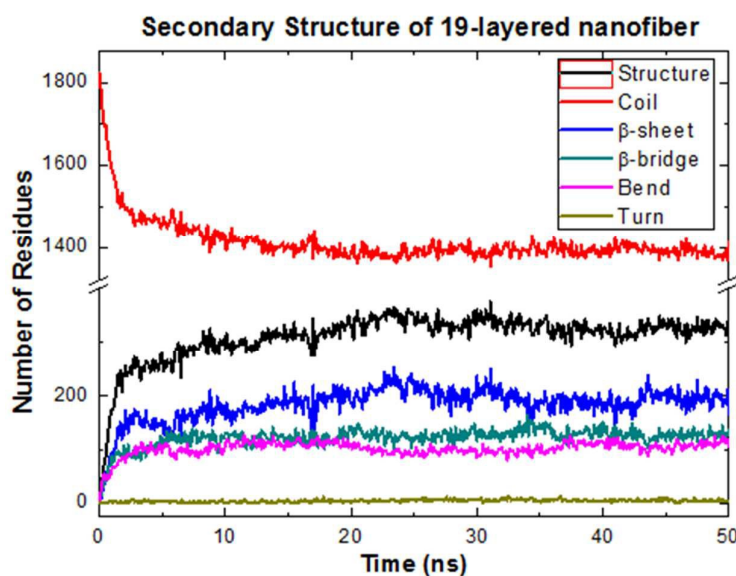


Figure 4: Plot of the number of residues forming secondary structure elements of the 19-layered nanofiber during the 50 ns MD simulation. (Structure= β -sheet+ β -bridge+Turn)

In our simulations, parallel β -sheets are formed between two adjacent PA molecules (Figure 5 and Figure S2) which is consistent with the data obtained from the CD spectra by Paramonov *et al.* [16]. That means, in the self-assembly mechanism of PAs, firstly dimers are formed, then dimers combine with single PAs to form trimers. This can be the first step for the aggregation which was also stated in our previous simulation [47]. The directions of the β -sheets are mostly radially outward.

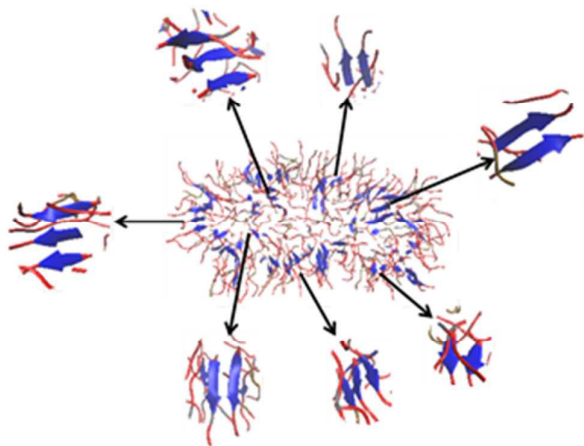


Figure 5: β -sheets in the self-assembled 19-layered fiber at the end of 50 ns simulation. Some of the dimers and trimers are zoomed in.

To get information about the hydrophobic and electrostatic interactions, the number of contacts in the fibers at a distance of less than 0.4 nm is calculated. In Figure 6 and Figure S3, we show the number of contacts as a function of time between the alkyl tails, between the VVAG peptide segments and between the alkyl tails and the VVAG segments. According to these results, the predominant hydrophobic interactions are between the VVAG peptide segments, the hydrophobic interactions between the alkyl tails are the second.

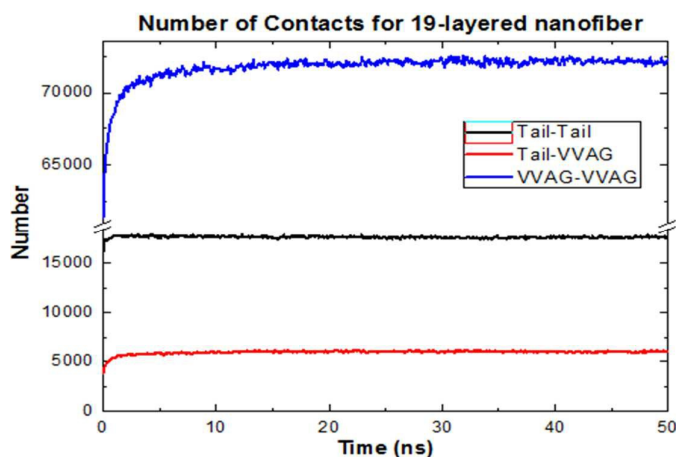


Figure 6: Hydrophobic interactions (number of contacts < 0.4 nm) of 19-layered nanofiber based on the alkyl tail and VVAG over the simulation time of 50 ns.

In Figure 7 and Figure S4, we show the number of contacts during the simulation time between the Na^+ ions and D, E, R residues, respectively and the most dominant interaction is between the D and Na^+ , since D has a negative charge of 2. In addition, the number of contacts between the D-R and between the E-R is calculated (Figure 7 and Figure S4). The most dominant electrostatic interaction is between the E (-1) and R (+1) residues as expected since they are closer to each other.

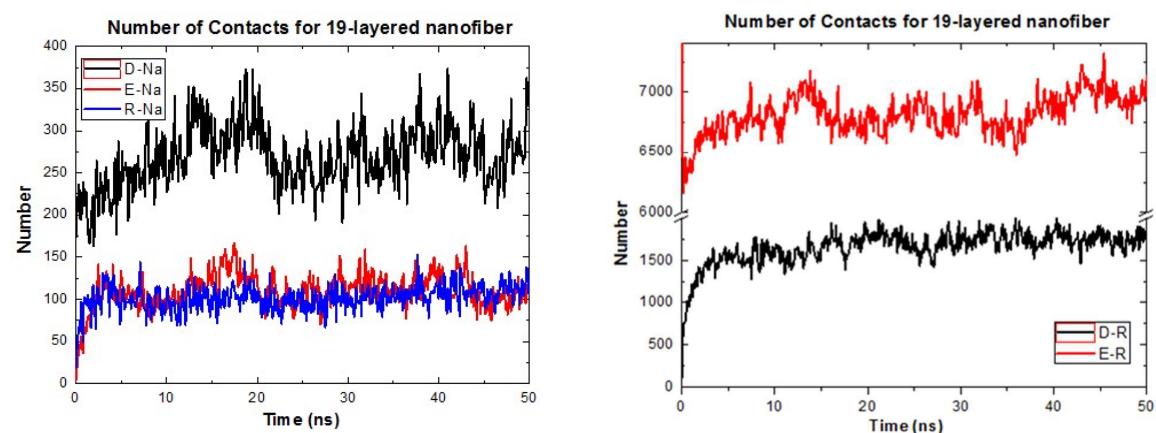


Figure 7: Electrostatic interactions (number of contacts $< 0.4 \text{ nm}$) of 19-layered nanofiber based on the residues D, E, R and Na ions over the simulation time of 50 ns.

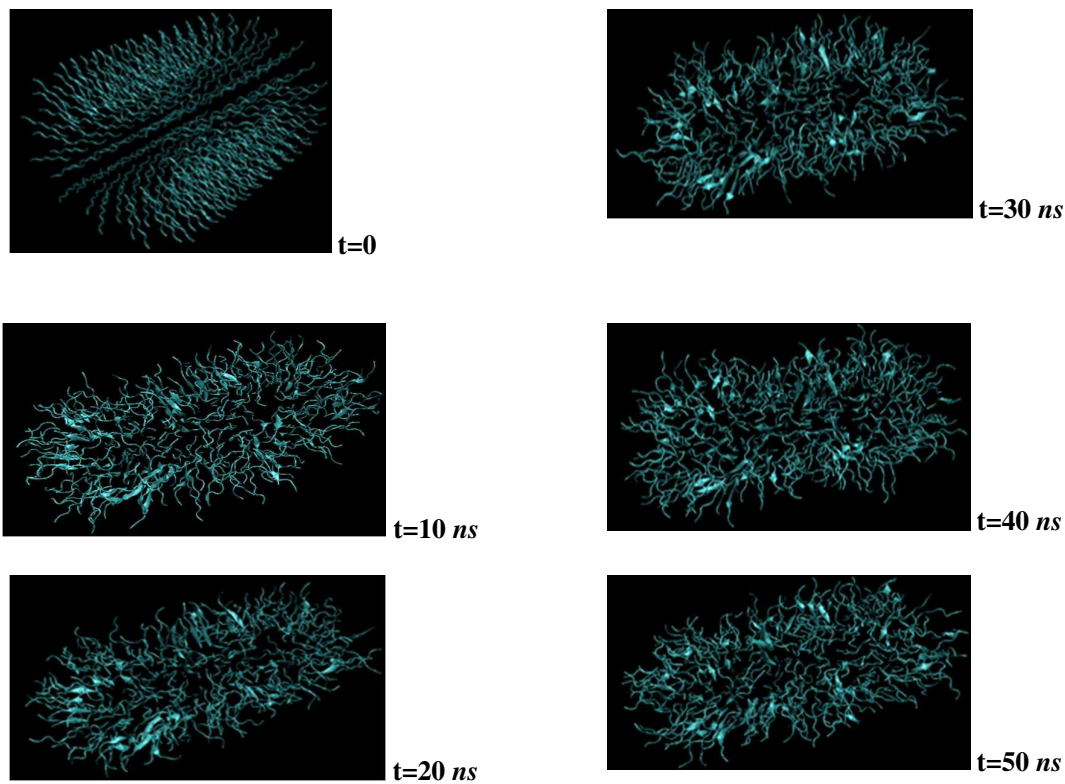


Figure 8: Snapshots of self-assembled 19-layered nanofiber for each 10 *ns* of 50 *ns* simulation.

Small-Angle X-ray Scattering (SAXS) analysis is another means of revealing the structure of the system. In Figure 9, we have depicted the Kratky plot of the SAXS data which confirms that the 19-layered structure remains intact after 50 *ns* simulation. The horizontal axis refers to the momentum transfer, while the vertical axis shows the product of the intensity times the square of the transferred momentum. The appearance of a distinct maximum is interpreted as the existence of a folded structure.

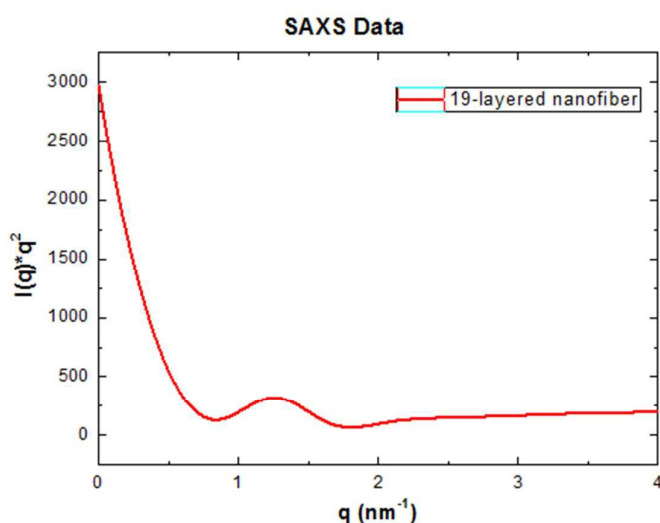


Figure 9: Kratky plot of the 19-layered structure

Table 2 summarizes the results of our computation. Nanofibers with RMSD values around 2 *nm* keep their structure intact, while the ones with larger values disintegrate. According to this prescription, after 30 or 50 *ns* simulation, 7,9,12 layered systems form a micelle, while 13,14,16,19 layered systems remain cylinders. 17, 18, 20, 21 layered systems disintegrate. Note that there is a direct correlation between the number of h-bonds and the RMSD values. R_g computation is in agreement with the RMSD results and specifically, the R_g value of the 19-layered structure with a radius of (about) 4.2 *nm* is also consistent with the results of the experiments [7, 21]. For all nanofibers, the DSSP analysis shows that, the most dominant secondary structure is random coil, followed by β -sheets. The table also shows the most dominant hydrophobic and electrostatic interactions.

Table 2: Summary of the Results

| # of layers | Average RMSD (nm) | Average Number of h-bonds | Average Rg (nm) | % of β -sheets | *Hydrophobic Interaction (VVAG-VVAG) | *Electrostatic Interaction (E-R) | *Electrostatic Interaction (D-Na) |
|-------------|-------------------|---------------------------|-----------------|----------------------|--------------------------------------|----------------------------------|-----------------------------------|
| 7 | 1.9 | 282 | 2.6 | 10 | 21906 | 1938 | 45 |
| 9 | 1.8 | 381 | 2.8 | 12 | 28160 | 2494 | 74 |
| 12 | 2.0 | 345 | 2.8 | 9 | 26242 | 2323 | 61 |
| 13 | 1.9 | 435 | 3.1 | 10 | 32516 | 2830 | 82 |
| 14 | 1.9 | 548 | 3.4 | 8 | 39537 | 3611 | 118 |
| 16 | 2.1 | 610 | 3.7 | 13 | 45014 | 4000 | 135 |
| 17 | 2.6 | 518 | 4.4 | 8 | 42155 | 3626 | 95 |
| 18 | 3.4 | 477 | 5.3 | 5 | 38968 | 3367 | 81 |
| 19 | 1.7 | 992 | 4.2 | 14 | 71766 | 6818 | 268 |
| 20 | 4.9 | 525 | 6.1 | 8 | 43280 | 3588 | 79 |
| 21 | 3.4 | 658 | 5.9 | 9 | 52202 | 4472 | 117 |

* # of the most dominant interactions.

CONCLUSIONS

We performed united-atom MD simulations to get a better understanding of self-assembly mechanism of PA-based (C₁₂-Val-Val-Ala-Gly-Glu-Arg-Gly-Asp) cylindrical nanofibers. Among the simulated nanofibers, according to the RMSD results and the snapshots, 7, 9 and 12-layered fibers take the form of a micelle, 13, 14, 16 and 19-layered fibers are still cylindrical nanofibers at the end of 50 *ns* simulations. The other fibers with 17, 18, 20, 21 layers disintegrate to two or more pieces within a very short period of time (0.5-1.0 *ns*). Out of all the structures, according to the RMSD and Rg results, 19-layered nanofiber with 12 PA molecules at each layer is the most stable structure. It has a diameter of about 8.4 *nm* which is consistent with some previous experiments. Our results suggest that the number of PAs in each layer and the number of layers in a fiber determine the stability in a non-trivial way. In all simulated fibers, even if the most dominant secondary structure is a random coil (mostly in the ERGD region), β -sheets are also observed (mostly in the VVAG region). 19-layered nanofiber has the highest population of β -sheet structures and the highest number of hydrogen bonds. In agreement with the experiments, in our simulations parallel β -sheets are formed between two adjacent PA molecules in the self-assembly mechanism. We observed that firstly dimers are formed, then dimers combine with the left alone PAs to form trimers. We also found that the hydrophobic interactions between VVAG and VVAG and the electrostatic interactions between D and Na⁺ and between E and R are the most important interactions for the stability of the self-assembled PA-based cylindrical nanofibers.

ACKNOWLEDGMENT

The author would like to thank M.O. Guler, A. Dana, M. Kaya and I. Guler for useful discussions. This work was supported by TUBITAK-CAREER grant no: 112T452. Numerical calculations reported in this paper were fully performed at TUBITAK ULAKBIM, High Performance and Grid Computing Center (TRUBA resources).

REFERENCES

- [1] Tekin, E. D. Odd-even effect on the potential energy of the self-assembled Peptide Amphiphiles. *Chem. Phys. Lett.* **2014**, 614, 204-206.
- [2] Cui, H.; Webber, M. J.; Stupp S. I. Self-Assembly of Peptide Amphiphiles: From Molecules to Nanostructures to Biomaterials. *Biopolymers: Peptide Science*. **2010**, 94, 1-18.
- [3] Toksoz, S.; Guler, M. O. Self-assembled peptidic nanostructures. *Nano Today*. **2009**, 4, 458-469.
- [4] Dagdas, Y. S.; Tombuloglu, A.; Tekinay, A. B.; Dana, A.; Guler, M. O. Interfiber interactions alter the stiffness of gels formed by supramolecular self-assembled nanofibers. *Soft Matter*. **2011**, 7, 3524-3532.
- [5] Vauthe, Y. S.; Santoso, S.; Gong, H. Y.; Watson, N.; Zhang, S. G. Molecular self-assembly of surfactant-like peptides to form nanotubes and nanovesicles. *Proc. Natl. Acad. Sci. U.S.A.* **2002**, 99, 5355-5360.
- [6] Behanna, H. A.; Donners, J.; Gordon, A. C.; Stupp, S. I. Coassembly of amphiphiles with opposite peptide polarities into nanofibers. *J. Am. Chem. Soc.* **2005**, 127:1193.
- [7] Hartgerink, J. D.; Beniash, E.; Stupp, S. I. Self-assembly and mineralization of peptide-amphiphile nanofibers. *Science*. **2001**, 1684-1688.
- [8] Tysseling, V. M.; Sahni, V.; Pashuck, E. T.; Birch, D.; Hebert, A.; Czeisler, C.; Stupp, S. I.; Kessler, J. A. Self-assembling peptide amphiphile promotes plasticity of serotonergic fibers following spinal cord injury. *J. Neurosci. Res.* **2010**, 88, 3161-3170.
- [9] Tysseling, V. M.; Sahni, V.; Niece, K. L.; Birch, D.; Czeisler, C.; Fehlings, M. G.; Stupp, S. I.; Kessler, J. A. Self-assembling nanofibers inhibit glial scar formation and promote axon elongation after spinal cord injury. *J. Neurosci.* **2008**, 28, 3814-3823.
- [10] Zhang, S. G. Fabrication of novel biomaterials through molecular self-assembly. *Nat. Biotechnol.* **2003**, 21, 1171-1178.

- [11] Ellis-Behnke, R. G.; Liang, Y. X.; You, S. W.; Tay, D. K. C.; Zhang, S. G.; So, K. F.; Schneider, G. E. Nano neuro knitting: Peptide nanofiber scaffold for brain repair and axon regeneration with functional return of vision. *Proc. Natl. Acad. Sci. U. S. A.* **2006**, 103, 5054-5059.
- [12] Capito, R. M.; Azevedo, H. S.; Velichko, Y. S.; Mata, A.; Stupp, S. I. Self-Assembly of Large and Small Molecules into Hierarchically Ordered Sacs and Membranes, *Science*, **2008**, 319, 1812-1816.
- [13] Silva, G. A.; Czeisler, C.; Niece, K. L.; Beniash, E.; Harrington, D. A.; Kessler, J. A.; Stupp, S. I. Selective Differentiation of Neural Progenitor Cells by High-Epitope Density Nanofibers. *Science*. **2004**, 303, 1352-1355.
- [14] Kunitake, T.; Nakashima, N.; Morimitsu, K. Enhanced Circular Dichroism and Fluidity of disk-like aggregates of a chiral, single-chain amphiphile. *Chem. Lett.* **1980**, 9, 1347-1350.
- [15] Gore, T.; Dori, Y.; Talmon, Y.; Tirrell, M.; Bianco-Peled, H. Self-Assembly of Model Collagen Peptide Amphiphiles. *Langmuir*. **2001**, 17, 5352-5360.
- [16] Paramonov, S. E.; Jun, H-W.; Hartgerink, J. D. Self-Assembly of Peptide-Amphiphile Nanofibers: The Roles of Hydrogen Bonding and Amphiphilic Packing. *J. Am. Chem. Soc.* **2006**, 128, 7291-7298.
- [17] Jiang, H.; Guler, M. O.; Stupp, S. I. The internal structure of self-assembled peptide amphiphiles nanofibers, *Soft Matter*, **2007**, 3, 454-462.
- [18] Toksoz, S.; Mammadov, R.; Tekinay, A. B.; Guler, M. O. Electrostatic effects on nanofiber formation of self-assembling peptide amphiphiles. *J. Colloid Interface Sci.* **2011**, 356, 131-137.
- [19] Hartgerink, J. D.; Beniash, E.; Stupp, S. I. Peptide-Amphiphile Nanofibers: a Versatile Scaffold for the Preparation of Self-Assembling Materials. *Proc. Natl. Acad. Sci. U.S.A.* **2002**, 99, 5133-5138.
- [20] Xu, X. D.; Jin, Y.; Liu, Y.; Zhang, X. Z.; Zhuo, R. X. Self-Assembly Behavior of Peptide Amphiphiles (PAs) with Different Length of Hydrophobic Alkyl Tails. *Colloids Surf. B: Biointerfaces* **2010**, 81, 329-335.
- [21] Pashuck, E. T.; Cui, H.; Stupp, S. I. Tuning Supramolecular Rigidity of Peptide Fibers Through Molecular Structure. *J. Am. Chem. Soc.* **2010**, 132, 6041-6046.

- [22] Missirlis, D.; Chworos, A.; Fu, C. J.; Khant, H. A.; Krogstad, D. V.; Tirrell, M. Effect of the Peptide Secondary Structure on the Peptide Amphiphile Supramolecular Structure and Interactions. *Langmuir*. **2011**, 27, 6163–6170.
- [23] Han, S.; Cao, S.; Wang, Y.; Wang, J.; Xia, D.; Xu, H.; Zhao, X.; Lu, J. R. Self-Assembly of Short Peptide Amphiphiles: the Cooperative Effect of Hydrophobic Interaction and Hydrogen Bonding. *Chem. Eur. J.* **2011**, 17, 13095–13102.
- [24] Zhang, S.; Gelain, F.; Zhao, X. Designer self-assembling peptide nanofiber scaffolds for 3D tissue cell cultures. *Semin. Cancer Biol.* **2005**, 15, 413-420.
- [25] Banwell, E. F.; Abelardo, E. S.; Adams, D. J.; Birchall, M. A.; Corrigan, A.; Donald, A. M.; Kirkland, M.; Serpell, L. C.; Butler, M. F.; Woolfson, D. N. Rational design and application of responsive α -helical peptide hydrogels. *Nat. Mater.* **2009**, 8, 596-600.
- [26] Guler, M. O.; Soukasene, S.; Hulvat, J. F.; Stupp, S. I. Presentation and Recognition of Biotin on Nanofibers Formed by Branched Peptide Amphiphiles, *Nano Lett.* **2005**, 5, 249-252.
- [27] Lee, O-S.; Stupp, S. I.; Schatz, G. C. Atomistic Molecular Dynamics Simulations of Peptide Amphiphile Self-Assembly into Cylindrical Nanofibers. *J. Am. Chem. Soc.* **2011**, 133, 3677-83.
- [28] Lee, O. S.; Cho, V.; Schatz, G. C. Modeling the Self-Assembly of Peptide Amphiphiles into Fibers Using Coarse-Grained Molecular Dynamics. *Nano Lett.* **2012**, 12, 4907–4913.
- [29] Lee, O-S; Liu, Y.; Schatz, G. C. Molecular dynamics simulation of β -sheet formation in self-assembled peptide amphiphile fibers. *J. Nanopart Res.* **2012**, 14, 936-942.
- [30] Velichko, Y. S.; Stupp, S. I.; Cruz, M. O. Molecular Simulation Study of Peptide Amphiphile Self-Assembly. *J. Phys. Chem. B.* **2008**, 112, 2326-2334
- [31] Fu, I. W.; Markegard, C. B.; Chu, B. K.; Nguyen, H. D. Role of Hydrophobicity on Self-Assembly by Peptide Amphiphiles via Molecular Dynamics Simulations. *Langmuir*. **2014**, 30, 7745–7754.
- [32] Niece, K. L.; Hartgerink, J. D.; Donners, J. J. J. M.; Stupp, S. I. Self-Assembly Combining Two Bioactive Peptide-Amphiphile Molecules into Nanofibers by Electrostatic Attraction. *J. Am. Chem. Soc.* **2003**, 125, 7146-7147.

- [33] Tsonchev, S.; Schatz, G. C.; Ratner, M. A. Hydrophobically-Driven Self-Assembly: A Geometric Packing Analysis, *Nano Lett.* **2003**, 3, 623-626.
- [34] Tsonchev, S.; Schatz, G. C.; Ratner, M. A. J. Electrostatically-Directed Self-Assembly of Cylindrical Peptide Amphiphile Nanostructures. *Phys. Chem. B.* **2004**, 108, 8817–8822.
- [35] Tsonchev, S.; Troisi, T.; Schatz, G. C.; Ratner, M. A. On the structure and stability of self-assembled zwitterionic peptide amphiphiles: a theoretical study. *Nano Lett.* **2004**, 4, 427–431.
- [36] Smith, P. E.; van Gunsteren, W. F. The viscosity of SPC and SPC/E water at 277 and 300K. *Chem. Phys. Lett.* **1993**, 215, 315–318.
- [37] Hess, B.; Kutzner, C.; van der Spoel, D.; Lindahl, E. GROMACS 4: Algorithms for Highly Efficient, Load-Balanced, and Scalable Molecular Simulation. *J. Chem. Theory Comp.* **2008**, 4, 435–447.
- [38] Oostenbrink, C.; Villa, A.; Mark, A. E.; van Gunsteren, W. A biomolecular force field based on the free enthalpy of hydration and solvation: the GROMOS force-field parameter sets 53A5 and 53A6. *J. Comput. Chem.* **2004**, 25, 1656-1676.
- [39] Berger, O.; Edholm, O.; Jähnig, F. Molecular dynamics simulations of a fluid bilayer of dipalmitoylphosphatidylcholine at full hydration, constant pressure, and constant temperature. *Biophys. J.* **1997**, 72, 2002-2013.
- [40] Parrinello, M.; Rahman, A. J. Polymorphic transitions in single crystals: A new molecular dynamics method. *J. Appl. Phys.* **1981**, 52, 7182–7190.
- [41] Bussi, G.; Donadio, D.; Parrinello, M. J. Canonical sampling through velocity rescaling. *Chem. Phys.* **2007**, 126, 014101–014107.
- [42] Hess, B.; Bekker, H.; Berendsen, H. J. C.; Fraaije, J. G. E. M. LINCS: a linear constraint solver for molecular simulations. *J. Comput. Chem.* **1997**, 18, 1463–1472.
- [43] Darden, T.; York, D.; Pedersen, L. J. Particle Mesh Ewald-an N.Log(N) method for Ewald sums in large systems. *Chem. Phys.* **1993**, 98, 10089–10092.

- [44] Verlet, L. Computer 'experiments' on classical fluids. I. Thermodynamical properties of Lennard-Jones molecules. *Phys. Rev.* **1967**, 159, 98–103.
- [45] Humphrey, W.; Dalke, A.; Schulten, K. J. VMD: visual molecular dynamics. *J. Mol. Graphics.* **1996**, 14, 33–38.
- [46] Kabsch, W.; Sander, C. Dictionary of protein secondary structure: pattern recognition of hydrogen-bonded and geometrical features. *Biopolymers.* **1983**, 22, 2577–2637.
- [47] Cinar, G.; Ceylan, H.; Urel, M.; Erkal, T. S.; Tekin, E. D.; Tekinay, A. B.; Dâna, A.; Guler, M. O. Amyloid Inspired Self-Assembled Peptide Nanofibers. *Biomacromolecules*, **2012**, 13, 3377–3387.